Monthly Notices
of the
ROYAL ASTRONOMICAL SOCIETY

MNRAS **479,** 130–140 (2018)
Advance Access publication 2018 June 1

doi:10.1093/mnras/sty1428

Solid deuterated water in space: detection constraints from laboratory experiments

R. G. Urso,[1,2★] M. E. Palumbo,[2★] G. A. Baratta,[2★] C. Scirè[2] and G. Strazzulla[2]

[1]*Dipartimento di Scienze Chimiche, Università degli Studi di Catania, Viale Andrea Doria 6, I-95125 Catania, Italy*
[2]*INAF-Osservatorio Astrofisico di Catania, via Santa Sofia 78, I-95123 Catania, Italy*

Accepted 2018 May 30. Received 2018 May 21; in original form 2017 December 21

ABSTRACT

The comparison between astronomical spectra and laboratory experiments is fundamental to spread light on the structure and composition of ices found in interstellar dense molecular clouds and in Solar system bodies. Water is among the most abundant solid-phase species observed in these environments, and several attempts have been made to investigate the presence of its solid-phase isotopologues. In particular, the detection of the O–D stretching mode band at 4.1 μm due to both D_2O and HDO within icy grain mantles is still under debate, and no detection has been reported about the presence of these species within icy bodies in the Solar system yet. In the near future, an important contribution could derive from the data acquired in the O–D stretching mode spectral range by the sensitive instruments on board the *James Webb Space Telescope*. With this in mind, we performed several laboratory experiments to study the O–D stretching mode band in solid mixtures containing water and deuterated water deposited in the temperature range between 17 and 155 K, in order to simulate astrophysical relevant conditions. Furthermore, samples have been studied at various temperature and irradiated with energetic ions (200 keV H^+) in order to study the effects induced by both thermal and energetic processing. Our results provide some constraints on the detection of the 4.1 μm band in astronomical environments.

Key words: astrochemistry – techniques: spectroscopic – ISM: abundances – infrared: ISM – infrared: planetary systems.

1 INTRODUCTION

Infrared observations toward star-forming regions allow to obtain primary information on the chemical and physical nature of dust grains and their icy mantles (e.g. Boogert, Gerakines & Whittet 2015). The analysis of the spectra acquired reveal the presence of water and carbon monoxide as the main constituents of icy grain mantles, followed by carbon dioxide, methane, methanol, and ammonia (Boogert, Schutte & Helmich 1997; Gibb et al. 2004; Dartois 2005; Öberg et al. 2011; Boogert et al. 2015). Also, other molecules have been likely detected, such as formaldehyde (H_2CO), sulphur dioxide (SO_2), and carbonyl sulphide (OCS, Schutte et al. 1994; Boogert et al. 1997; Palumbo, Geballe & Tielens 1997). Solid phase molecules are also present on a variety of places in the Solar system, such as on the surfaces of satellites of outer planets, the trans-Neptunian objects (such as Pluto), and the comets (e.g. Cruikshank, Veverka & Lebofsky 1984; Morrison et al. 1984; Thomas, Veverka & Dermott 1986; Brown et al. 1995; Calvin, Clark & Brown 1995; Cruikshank et al. 1995; Nash & Betts 1995).

To better understand the chemical composition and physical structure of ices in space, it is fundamental to compare infrared spectra acquired by telescopes with those obtained in laboratory experiments in which ice analogues are produced. As an example, several experimental works have been focused on studying thermal induced changes in water ice by means of laboratory infrared spectroscopy. The study of the band profiles (i.e. shape, width, and peak position) with increasing temperature allowed to obtain information about the physical structure of water ice and its phase changes (e.g. Hudgins et al. 1993; Grundy & Schmitt 1998; Dartois & d'Hendecourt 2001; Bossa et al. 2012).

In particular, the 3 μm band profile of solid water, related to both symmetric and asymmetric O–H stretching vibrational modes, shows a strong variation with increasing temperature. In fact, at low temperature (few tens K)À, it appears smooth and symmetric. During the warm up, the band profile gradually changes between 100 and 155 K, becoming sharper and structured. Detailed studies on this feature attributed the change to both porosity diminution of the as deposited sample (e.g. Bossa et al. 2012) and its transition between a disordered phase to a much ordered one, i.e. amorphous to crys-

★ E-mail: rurso@oact.inaf.it (RU); maria.palumbo@inaf.it (MP); giuseppe.baratta@inaf.it (GB)

talline transition (e.g. Rowland, Fisher & Devlin 1991; Jenniskens & Blake 1994). The change in porosity is also testified by the disappearance of the O–H dangling bond feature, that is characterized by the presence of the two bands centred at 3697 and 3720 cm^{-1}, attributed to three- and two-coordinated water molecules, respectively, that appear in porous amorphous water ice only (e.g. Rowland et al. 1991; Palumbo 2006).

The search for structural variations has been carried out for other astrophysical relevant species. Hudgins et al. (1993) reported about the infrared spectra of several species and mixtures with increasing temperature. As an example, they observed that the methanol amorphous-to-crystalline transition takes place between 100 and 120 K, as evidenced by the sharpening of its infrared bands. Recently, Urso et al. (2017) have shown experimental results on the thermal evolution of solid state formamide between 17 and 300 K. Also in this case, the warm up induce the crystallization of the formamide sample, which is evidenced by the sharpening of all the formamide vibrational features.

Together with thermal processing and energetic processing, i.e. bombardment by cosmic rays and UV photons, has a strong effect in modifying the chemical and physical structure of ices. In particular, laboratory experiments have shown that one of the most evident effects induced by energetic processing is the ice compaction and amorphization. As an example, it has been shown that ion bombardment causes both the compaction of amorphous water ice (e.g. Palumbo 2006; Raut et al. 2007; Dartois et al. 2013) and the amorphization of crystalline water ice (e.g. Baratta et al. 1991; Moore & Hudson 1992; Leto & Baratta 2003; Leto et al. 2005; Dartois et al. 2015). Taking into account the differences observed in the band profiles of amorphous and crystalline samples acquired in laboratory experiments, it has been possible to spread light on the icy grain mantles structure in the star-forming regions (e.g. Dartois & d'Hendecourt 2001) and on outer Solar system objects (e.g. Grundy et al. 1999).

Several water and carbon monoxide isotopologues have been detected in the gas phase of star-forming regions, such as HDO, $H_2{}^{18}O$, D_2O, $^{13}C^{18}O$, ^{13}CO, $C^{17}O$, and $C^{18}O$ (e.g. Turner et al. 1975; Jacq et al. 1988; Langer & Penzias 1990; Butner et al. 2007; Pineda, Caselli & Goodman 2008; Kama et al. 2013; Coutens et al. 2014; Nagy et al. 2017). In the solid-phase, ^{13}CO has been detected, together with $^{13}CO_2$ (e.g. Boogert et al. 2000; Boogert, Blake & Tielens 2002; Gibb et al. 2004). In 1999, the detection of solid HDO was claimed by Teixeira et al. (1999) that reported about the presence of the O–D stretching mode band at 4.1 μm in the line of sight to the high-mass protostars W33 A and NGC 7538 IRS9 thanks to the comparison between *ISO*–SWS spectra and laboratory infrared spectra of solid mixtures containing various ratios of water and deuterated water. However, these detections have been questioned by Dartois et al. (2003). In fact, thanks to the comparison between laboratory experiments and spectroscopic observations carried out with two telescopes (VLT and UKIRT) towards both high- and intermediate mass protostars, they report that the HDO 4.1 μm feature detected towards W33 A by Teixeira et al. (1999) could be due to calibration and instrumental response problems. Also, they point out that the HDO identification is affected by the methanol vibrational mode bands that are found at these wavelengths. Furthermore, the HDO absorption in NGC 7538 IRS9 reported by Teixeira et al. (1999) could be attributed to detector instabilities. Also Parise et al. (2003) searched for solid HDO towards low-mass protostars. They did not detect this species in any of the investigated sources, and they gave upper limits from 0.5 to 2 per cent for the HDO/H_2O ratio. Recently, Aikawa et al. (2012) reported about the tentative detection

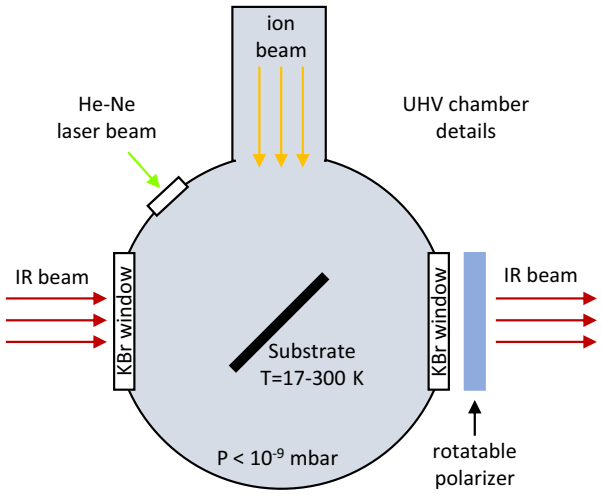

Figure 1. Schematic top view of the UHV chamber and the geometry used to perform irradiation and infrared spectroscopy on frozen samples.

of the O–D stretching mode in HDO towards the protostellar objects L1527, IRC-L1041, IRAS04302, and HV Tau obtained with the infrared camera on board of the *AKARI* telescope. Using the band strength value determined by Dartois et al. (2003; 4.3×10^{-17} cm $molecule^{-1}$), they calculated the HDO abundance between 2 and 22 per cent w.r.t. H_2O.

In the Solar system, gas-phase isotopologues have been observed (e.g. Hartogh et al. 2011; Altwegg et al. 2015, 2017; Füri & Marthy 2015), while to the best of our knowledge, the detection of solid-phase isotopologues has not yet been reported.

Useful data on the presence and abundance of solid-phase deuterated water in space could be obtained by *James Webb Space Telescope (JWST)* observations. In fact, the sensitivity of the on-board detectors could allow the detection of the 4.1 μm band. With this in mind, in this work we describe recent experiments we performed to study the O–D stretching mode band in solid mixtures containing water and deuterated water in various ratios and temperatures. During the experiments, the samples have been deposited in the temperature range between 17 and 155 K, in order to simulate astrophysical relevant conditions. Furthermore, samples have been studied at various temperature and irradiated with energetic ions (200 keV H^+) in order to study the effects induced by both thermal and energetic processing. The implications to the detectability of this band in astrophysical environments are discussed.

2 EXPERIMENTAL METHODS

The experiments were performed in the Laboratory for Experimental Astrophysics at INAF-Osservatorio Astrofisico di Catania (Italy). Two different sets of experiments were performed in order to investigate the thermal evolution and the effects of the bombardment with energetic ions (200 keV H^+) on frozen mixtures containing H_2O, HDO, and D_2O. The experiments were performed in an ultra-high vacuum (UHV) chamber ($P\leq 10^{-9}$ mbar, see Fig. 1) in which a KBr substrate is placed in thermal contact with the cold finger of a closed-cycle helium cryocooler (CTI) for which temperature can be varied between 17 and 300 K. Gaseous mixtures were prepared in a mixing chamber in which pure water (Sigma Aldrich Chromasolv Plus) and D_2O (Aldrich, 99.990 per cent D) are injected. In this chamber, mixtures with various H_2O/D_2O ratios were prepared, and for each mixture we waited enough to allow the isotopic exchange

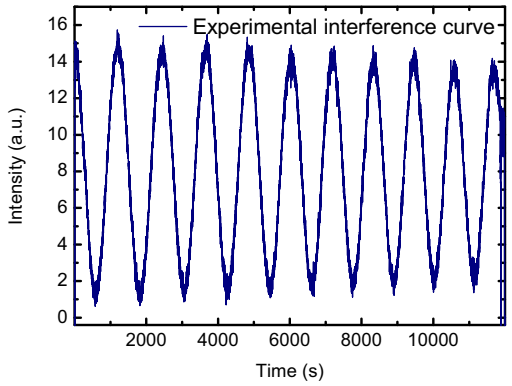

Figure 2. Experimental interference curve obtained using a He–Ne laser during the deposition of a D_2O:HDO =3:1 mixture on a KBr substrate.

between H_2O and D_2O to occur. A needle valve allows the resulting mixtures to enter the UHV chamber, where they condense on the cold substrate forming a solid film. The gas inlet is not faced to the substrate, allowing the background deposition of mixtures.

The frozen mixture ratios have been calculated a posteriori from the infrared spectra obtained after each deposition, measuring the O–H and O–D stretching mode band areas. To estimate the column density N of water and deuterated water in the samples we used the equation ,

$$N = \frac{\int \tau_\nu d\nu}{A}, \quad (1)$$

where τ_ν is the optical depth and A is the band strength (cm molecule^{-1}). For the O–H stretching mode band $A = 2.0\times 10^{-16}$ cm molecule^{-1} (Gerakines et al. 1995), while for the O–D stretching mode band $A = 4.3\times 10^{-17}$ cm molecule^{-1} (Dartois et al. 2003). The resulting mixtures are H_2O:HDO = 1000:1, H_2O:HDO = 2:1, and D_2O:HDO = 3:1. The complete isotopic exchange between H_2O and D_2O in the mixing chamber is confirmed by the band profile in the infrared spectra. In fact, as shown by Gálvez et al. (2011), when both HDO and D_2O are present, the profile of the O–D stretching band shows two overlapping components which are not observed in our spectra. Similarly, we are confident that no H_2O is present in the mixture D_2O:HDO = 3:1.

During the deposition, the accretion of the film has been measured by looking at the interference curve (intensity versus time) of a reflected laser beam (He–Ne, λ = 543.5 nm), following the procedure described in Fulvio et al. (2009) and Urso et al. (2016). Fig. 2 represents the deposition of 10 fringes of a D_2O:HDO = 3:1 solid mixture.

To study the sample thermal evolution, mixtures were deposited at 17 K and warmed up to their complete desorption. Temperature is measured with a silicon diode, placed close to the sample holder, with an accuracy of ±1 K and is stabilized within ±0.1 K. Several steps of warm up were performed for each sample. In the case of the energetic processing experiments, the mixtures were irradiated with 200 keV H^+ at 17 K. The UHV chamber is connected to a 200 kV ion implanter by Danfysik. The electrostatical sweeping of the ion beam ensures the uniform coverage of the target, and the ion current density between 100 nA cm^{-2} and a few μA cm^{-2} prevents its macroscopic heating. The integration of the ion current during the irradiation allows to measure the ion fluence (ions cm^{-2}). The energy deposited by incoming ions to the sample (dose) was calculated using the stopping power given by the SRIM code (Ziegler, Biersack & Ziegler 2008) and following the procedure described in (Urso et al. 2017). The dose is given in eV/16u, a convenient way to characterize chemical and physical changes, and to allow a comparison with other irradiation experiments (Strazzulla & Johnson 1991).

Infrared transmission spectroscopy was used to analyse the samples. Spectra were collected at oblique incidence (45°) with a Bruker Vertex 70 Fourier transform infrared (FTIR) spectrometer (resolution = 1 cm^{-1}, sampling = 0.25 cm^{-1}) equipped with a rotatable polarizer along the path of the IR beam. The polarizer allows acquiring of the spectra with the electric vector both parallel and perpendicular to the plane of incidence of the infrared beam, i.e. in P- or S-polarization. Background P- and S-polarization spectra of the bare cold substrate were acquired before ice deposition. We collected spectra of the samples as deposited and after each step of irradiation and warm up. Each sample spectrum is ratioed to the background spectrum acquired in the same polarization mode. Unless differently specified, here we show the spectra acquired in P-polarization because of a better signal-to-noise ratio.

3 RESULTS

In this section we present experimental results on the thermal processing of samples investigated in this work. Spectra (Figs 3–5) have been collected at 17, 40, 80, 110, 120, 130, 140, and 155 K, the latter being the crystallization temperature of water in our experimental conditions. For clarity, we show only the spectra acquired at 17, 140, and 155 K between 4200 and 500 cm^{-1} (2.4–20 μm) in transmittance scale. Top axes report the wavelength in μm and bottom axes the wavenumber in cm^{-1}. Table 1 reports the main vibrational modes identified in mixtures H_2O:HDO = 1000:1, D_2O:HDO = 3:1, and H_2O:HDO = 2:1 at 17 and 155 K. Also, in Section 3.3 we show the results of the energetic processing with 200 keV H^+ of H_2O:HDO = 1000:1 (Fig. 7) and H_2O:HDO = 2:1 mixture (Fig. 9).

3.1 Thermal processing of H_2O:HDO = 1000:1 mixture

In Fig. 3 we show the spectra acquired on a H_2O:HDO = 1000:1 frozen mixture. Panel A shows the spectra acquired at 17 (black line), 140 (red dashed line), and 155 K (blue dotted line). The narrowing and increasing in intensity of the O–H feature caused by warm up to 140 K, together with the absence of the O–H dangling bonds feature (see the inset in the figure), suggest that the sample experienced a diminution of porosity. Finally, at 155 K the whole spectrum depicts a less porous and crystalline water ice sample and the O–H stretching modes band exhibits three components (Hudgins et al. 1993; Bossa et al. 2012). The appearance of sub components in the O–H stretching mode band is due to the interaction between water molecules via H-bond. Different vibrational frequencies are ascribed to different types of local hydrogen bonding (e.g. Sun 2013). In Panel B the spectral range of the O–D stretching mode of HDO is shown. Within the noise of the spectrum, no feature is detectable in this frequency range at 17 K. A feature assigned to the O–D stretching mode band appears at about 80 K. In the spectrum acquired at 140 K it is centred at about 2440 cm^{-1}, while at 155 K it is narrower and shifted to about 2425 cm^{-1}.

3.2 Thermal processing of D_2O:HDO = 3:1 and H_2O:HDO = 2:1 mixtures

To better investigate the O–D stretching mode band profile, other experiments have been performed by depositing solid mixtures con-

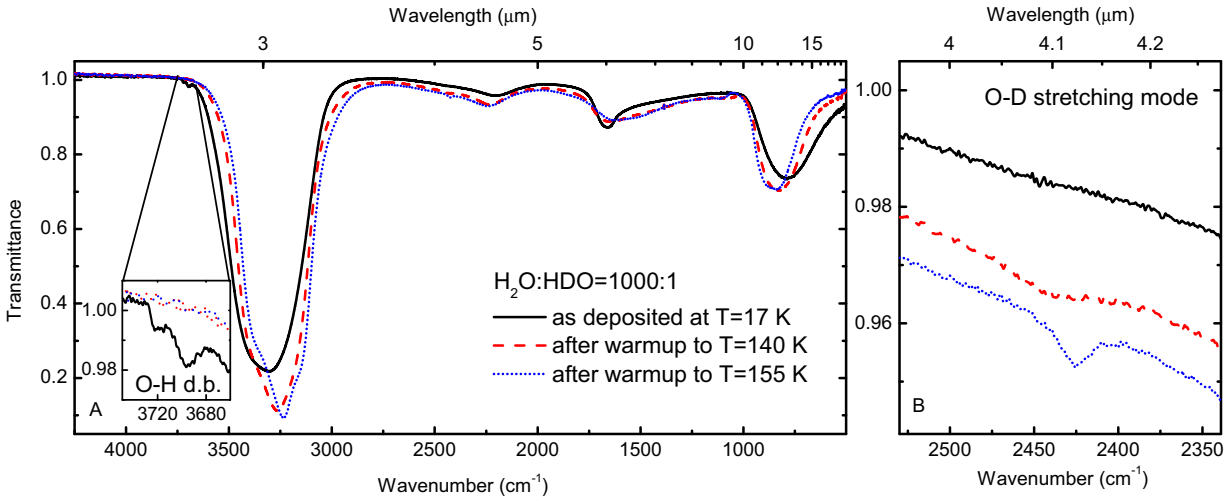

Figure 3. Infrared spectra in transmittance scale of H_2O:HDO = 1000:1 frozen mixture acquired at 17 (black line), 140 (red dashed line), and 155 K (blue dotted line) in transmittance scale. Panel A: full spectra; Inset: O–H dangling bonds feature; Panel B: O–D stretching modes region.

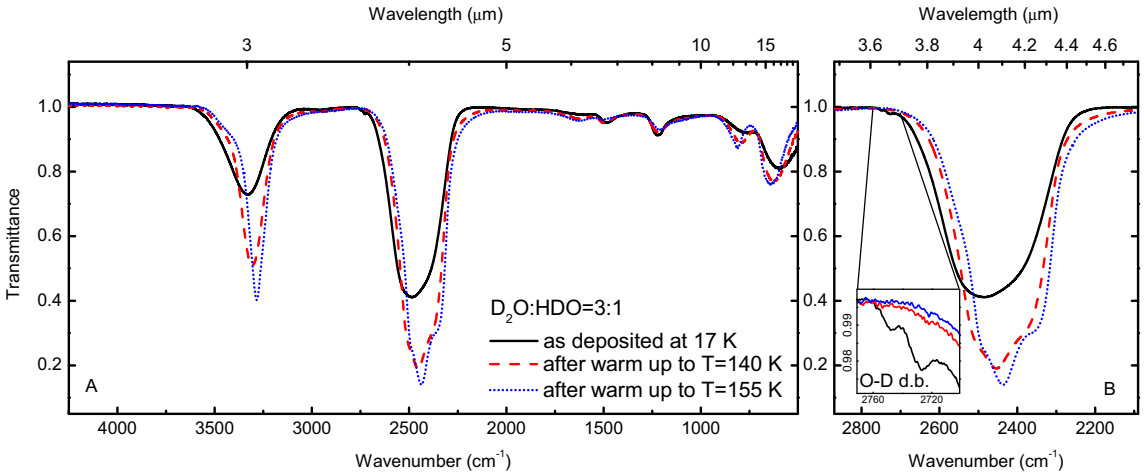

Figure 4. Infrared spectra in transmittance scale of a D_2O:HDO =3:1 mixture acquired at 17 (black line), 140 (red dashed line), and 155 K (blue dotted line). Panel A: full spectra; panel B: O–D stretching mode band; Inset in panel B: zoom on the O–D dangling bond feature.

taining a higher amount of deuterated water. In Fig. 4 the spectra of the D_2O:HDO = 3:1 mixture deposited at 17 K and warmed up to 140 and 155 K are shown.

At the deposition temperature (black line), the O–H stretching mode band is centred at 3331 cm^{-1} and the O–D stretching mode band at 2485 cm^{-1}. For both features, the warm up determines the shift towards shorter wavenumbers (see Table 1), the narrowing and the increase in intensity. These changes can be compared to those observed during the warm up experiment of H_2O:HDO = 1000:1 mixture. In particular, it is interesting to notice that the O–D stretching mode band (Fig. 4 panel B) follows the same behaviour observed for the 3300 cm^{-1} O–H stretching band in water (see Fig. 3). Also in this case we attribute these band profile changes to the sample diminution of porosity and to its amorphous-to-crystalline transition. It has to be noticed that the absence of the O–H dangling bond feature in the spectrum is acquired at 17 K, while we observed the O–D dangling bond bands (see the inset in Fig. 4, panel B), centred at 2727 and 2748 cm^{-1}. As already observed for the O–H dangling bond feature, these bands are not present in the spectra acquired at 140 and 155 K, confirming that the sample has been deposited as a porous film and that the heating caused the diminution of porosity.

We also performed another experiment by depositing a H_2O:HDO = 2:1 mixture. The spectra acquired at 17, 140 and 155 K are shown in Fig. 5. At 17 K, the O–H and the O–D stretching mode band are centred at 3319 cm^{-1} and 2459 cm^{-1}, respectively. As noticed in the previous experiments, for both bands a narrowing and increase in intensity is also observed, together with the shift towards shorter wavenumbers (see Table 1). It has to be noticed that the O–D dangling bond feature does not appear at the deposition temperature (see Fig. 5 panel B), where only the O–H dangling bonds bands are visible, centred at 3692 and 3718 cm^{-1}. This is due to the lower amount of as deposited deuterated water within the mixture with respect to the previous experiment.

In Fig. 6 we show the normalized O–D and O–H stretching mode band areas as a function of temperature. Panel A shows that in the H_2O:HDO = 1000:1 mixture, the O–D stretching mode can be observed approaching the amorphous-to-crystalline transition. Only upper limits can be established at temperature lower than 80 K. As it can be observed in panels B and C, when the deuterated

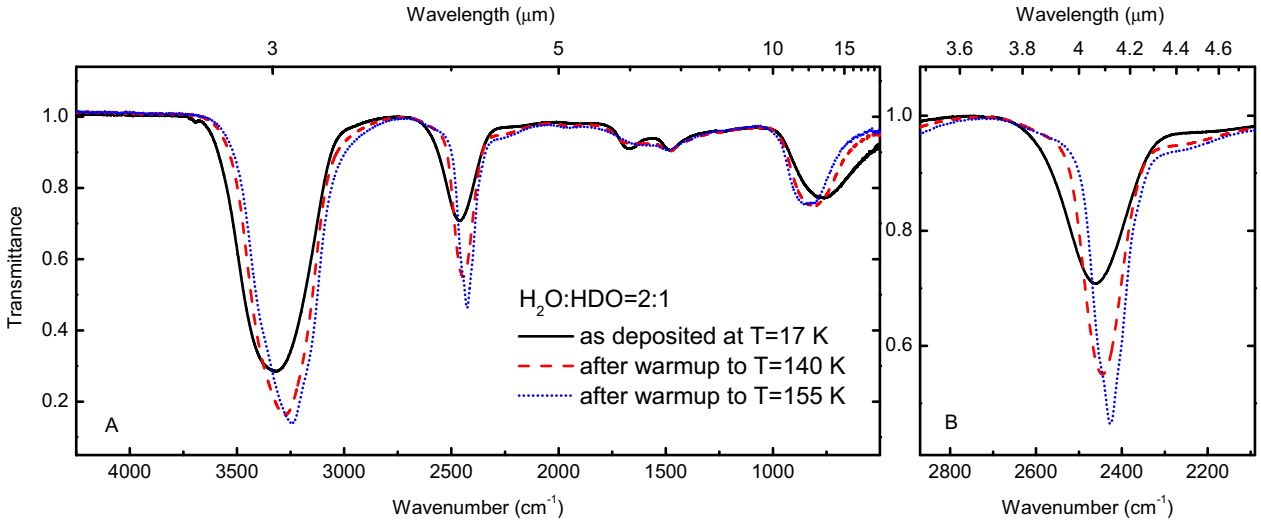

Figure 5. Infrared spectra in transmittance scale of a H_2O:HDO =2:1 mixture acquired at 17 (black line), 140 (red dashed line), and 155 K (blue dotted line). Panel A: full spectra; Panel B: O–D stretching mode band.

Table 1. Main vibrational modes of each species identified in mixtures H_2O:HDO = 1000:1, D_2O:HDO = 3:1, and H_2O:HDO = 2:1 at 17 and 155 K. Peak positions and full width at half-maximum (FWHM) are given in cm^{-1}. ν_1, ν_3: symmetric and asymmetric stretching modes; ν_2: bending mode; L_2: libration mode; -: absent. References used for the attributions: Hudgins et al. (1993); Palumbo (2006); Öberg et al. (2007); Gálvez et al. (2011). Due to the overlapping of H_2O and HDO L_2 modes in the mixture H_2O:HDO = 2:1, only one peak position and FWHM can be measured in the spectra. [a] and [b] refer to O–D and O–H stretching mode band position of HDO, respectively.

		H_2O:HDO = 1000:1		D_2O:HDO = 3:1		H_2O:HDO = 2:1	
Vibrational modes	(cm^{-1})	17 K	155 K	17 K	155 K	17 K	155 K
ν_1, ν_3 H_2O	peak	3312	3236	–	–	3319	3241
	FWHM	325	252	–	–	303	223
ν_1, ν_3 HDO	peak	–	2425[a]	3331[b]	3284[b]	2459	2426
	FWHM	–	21	204	86	194	74
ν_1, ν_3 D_2O	peak	–	–	2485	2436	–	–
	FWHM	–	–	249	188	–	–
ν_2 H_2O	peak	1659	1619	–	–	1670	1660
	FWHM	229	485	–	–	95	–
ν_2 HDO	peak	–	–	1478	1507	1481	1486
	FWHM	–	–	71	68	76	–
ν_2 D_2O	peak	–	–	1220	1209	–	–
	FWHM	–	–	79	118	–	–
L_2 H_2O	peak	788	837	–	–	759	828
	FWHM	295	210	–	–	286	207
L_2 HDO	peak	–	–	766	810	–	
	FWHM	–	–	92	61	–	
L_2 D_2O	peak	–	–	592	654	–	–
	FWHM	–	–	154	110	–	–

water/water ratio increases, the O–D stretching mode band can be detected at lower temperatures also, independently of the sample structural phase. Our results show that the ratio between the O–H and O–D features strongly depend on the temperature in the case of the HDO diluted mixture (panel A in Fig. 6), while it is independent of temperature when a high deuterium amount is considered (see panels B and C in Fig. 6). The behaviour of the O–D stretching mode band intensity in the diluted mixture is related to the distribution of nearest neighbour oxygen–oxygen distances; as a consequence, the band profile is broad for an amorphous sample and becomes narrow with the crystallization (e.g. Madden et al. 1978; Gálvez et al. 2011).

3.3 Energetic processing

In this section we report the results obtained during the irradiation experiments with 200 keV H^+. In the first experiment we deposited the H_2O:HDO = 1000:1 mixture at 155 K (Fig. 7, black line), then we cooled down the sample to 17 K. This experiment was performed to verify that the behaviour of the O–D feature is due to the sample phase change and not to temperature variations. At 155 K the sample is deposited in the crystalline phase (see Leto & Baratta 2003). After the spectrum acquisition, we cooled down the sample to 17 K (blue dashed line). The cooling determines the O–D stretching modes band shift from 2423 to 2412 cm^{-1} (see Fig. 7 panel C). The green dotted line in Fig. 7 shows the ice spectrum after

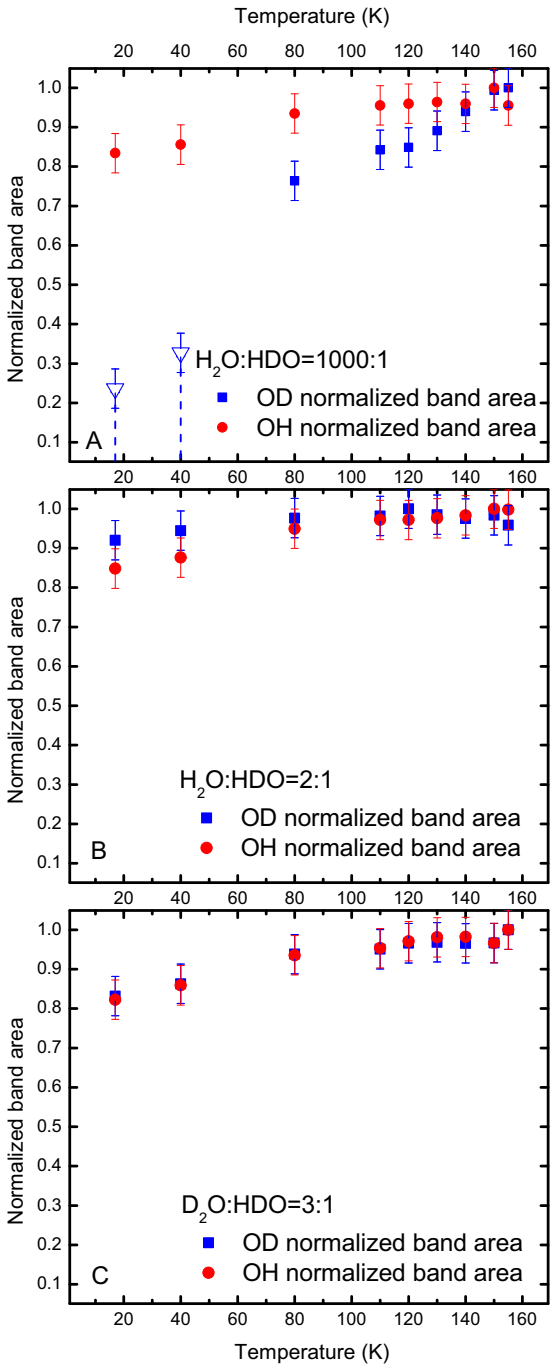

Figure 6. Normalized O–D and O–H stretching mode band areas as a function of temperature. Panel A: H_2O:HDO =1000:1; triangles and vertical dashed lines indicate upper limits for the measure; Panel B: H_2O:HDO =2:1 mixture; Panel C: D_2O:HDO =3:1.

the irradiation with 200 keV H^+ performed at 17 K. In particular, in Fig. 7 panel B it is possible to see that the O–H stretching mode band profile changed, becoming larger and decreasing in intensity. These changes testify that the irradiation caused the amorphization of the as deposited crystalline sample (e.g. Baratta et al. 1991; Leto & Baratta 2003; Dartois et al. 2015). After the irradiation, the O–D stretching modes band disappears because of the ion-induced amorphization. The warm up to 155 K induce the re-crystallization of the sample (red dot–dashed line), and the O–D feature appears again, centred at the same position it has been found in the as deposited sample.

In Fig. 8 we show the O–D and O–H band areas normalized to the initial value as a function of irradiation dose that we measured in the H_2O:HDO = 1000:1 frozen mixture. The O–D experimental data were fitted with an exponential curve $y=e^{-\sigma D}$, where σ is the cross section of the process in 16u/eV and D is the dose in eV/16u. The fit allows to obtain the cross section $\sigma = 1.3\pm0.1$ in 16u/eV.

Another experiment has been performed on a H_2O:HDO = 2:1 solid mixture deposited and irradiated at 17 K. The spectra acquired are shown in Fig. 9. The most intense bands are the O–H stretching mode of water and the O–D stretching mode of deuterated water. At 17 K, the sample is deposited as a porous and amorphous film, as testified by the presence of the O–H dangling bonds bands at 3692 and 3720 cm^{-1} in the spectrum acquired immediately after the deposition (black line, see the inset in Fig. 9 panel A). As expected, the irradiation with 200 keV H^+ caused the disappearance of the O–H dangling bond feature since the first irradiation step (red dashed line in the figure), thus compaction took place (e.g. Palumbo 2006; Raut et al. 2007; Dartois et al. 2013).

It is known that the ion irradiation of water induce the formation of hydrogen peroxide (e.g. Moore & Hudson 2000; Strazzulla et al. 2003; Zheng, Jewitt & Kaiser 2006). H_2O_2 exhibit a vibrational feature at about 2850 cm^{-1} ($\sim$3.5 μm). In the inset in Fig. 9 panel B the feature attributed to H_2O_2 found in the acquired spectra is shown. We did not find any evidence of HDO_2 nor D_2O_2 formation. In fact, excluding the H_2O_2 feature and a small contribution due to CO_2 contamination found at about 2340 cm^{-1}, the spectra acquired before and after irradiation are superimposable.

3.4 Other vibrational features in the 4.1 μm spectral range

The O–D feature falls in a region of the infrared spectrum where other astrophysically relevant species exhibit vibrational modes. A few examples are reported in Fig. 10, where spectra collected in the experimental setup described in Section 2 are shown. Red dashed line shows the O–D stretching mode band in the crystalline H_2O:HDO = 1000:1 mixture, while the purple dotted line shows the H_2O:HDO = 2:1 mixture at 17 K. Close to the O–D stretching mode band of deuterated water, both amorphous (black dashed line) and crystalline (blue dotted line) methanol (CH_3OH) exhibit a combination mode band at about 2450 cm^{-1} (e.g. Allamandola, Sandford & Tielens 1992; Sandford & Allamandola 1993; Bennett, Chen & Sun 2007). In star-forming regions, its abundance varies from a few per cent up to 30 per cent w.r.t. water (e.g. Allamandola et al. 1992; Boogert et al. 2008). Also sulphur dioxide (SO_2) exhibits a combination mode at about 2460 cm^{-1} (green line, Giguère & Falk 1956; Wiener & Nixon 1956). Boogert et al. (1997) reported that its abundance spans between 0.3 per cent and 0.8 per cent w.r.t. water. For each species we scaled the spectra taking into account the band intensities observed toward W33 A, according to the detections reported by Allamandola et al. (1992), Boogert et al. (1997), and Teixeira et al. (1999).

Finally, Fig. 11 shows a comparison between the profile of the O–D stretching mode band in a H_2O:HDO = 2:1 frozen mixture acquired both in P- and S-polarization. Within experimental uncertainties, the two profiles are perfectly superimposable. This condition is verified for the O–D stretching mode band in all the astrophysically relevant mixtures investigated in this work. As discussed by Baratta et al. (2000) and Palumbo & Baratta (2000), when the band profile does not depend on the polarization mode at oblique incidence, laboratory transmittance spectra of thin films are representative of

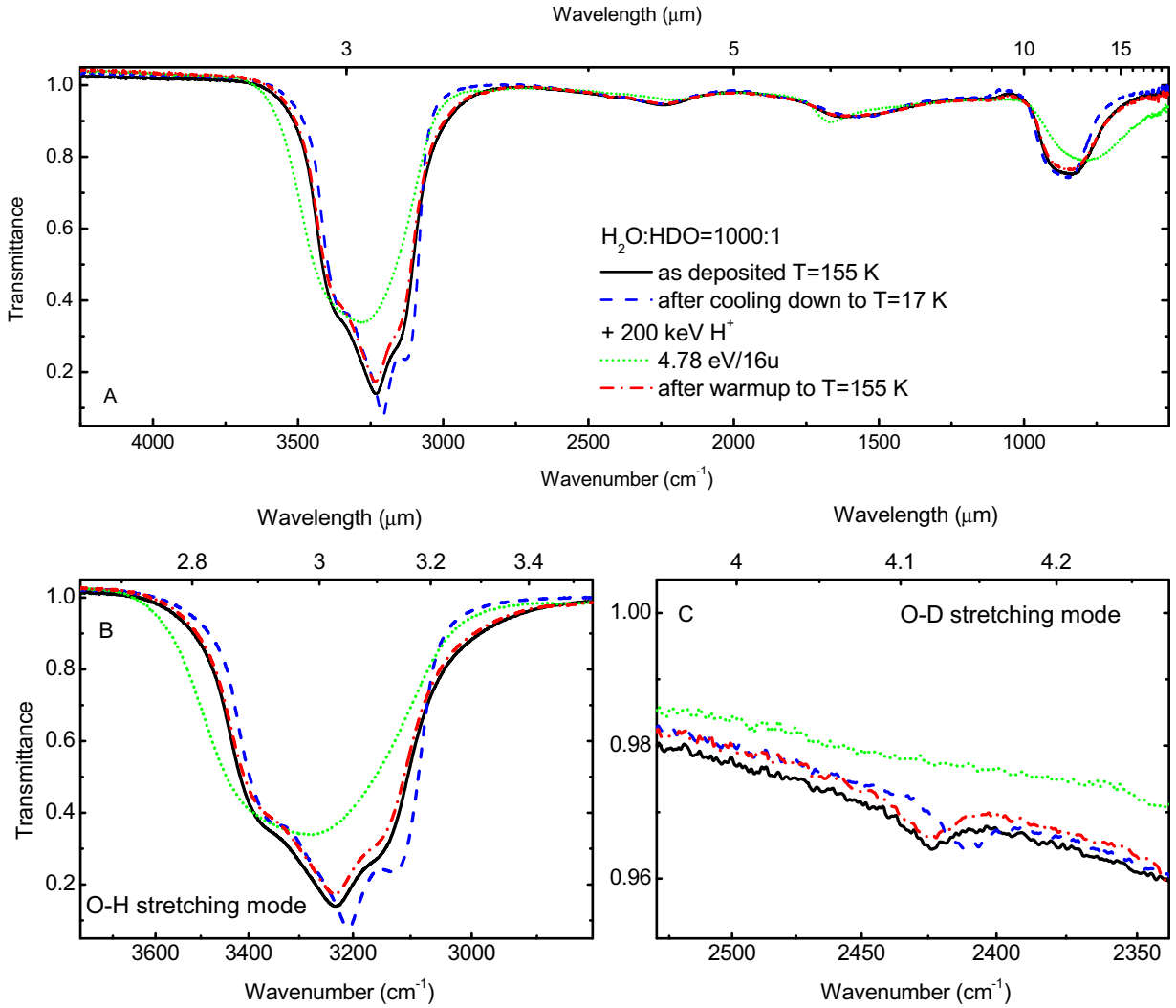

Figure 7. Infrared spectra in transmittance scale acquired during the irradiation experiments of crystalline H_2O:HDO =1000:1 with 200 keV H^+. Panel A: whole spectra; Panel B: O–H stretching mode band; panel C: O–D stretching mode band.

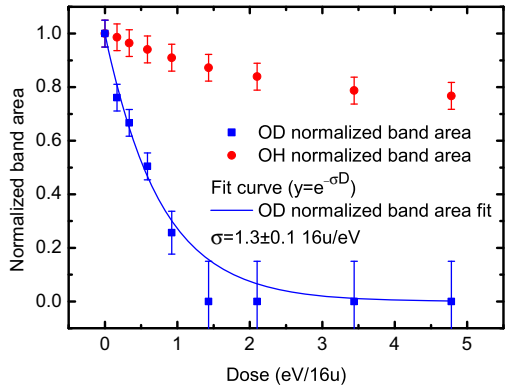

Figure 8. O–D and O–H features normalized areas after ion irradiation with 200 keV H^+ of a H_2O:HDO =1000:1 solid mixture at 17 K. The O–D experimental data have been fitted with an exponential curve $y=e^{-\sigma D}$, where σ is the cross section in 16u/eV and D is the dose in eV/16u.

small particles extinction cross section and surface modes are negligible. Hence, a direct comparison between laboratory spectra and astronomical observations is possible.

4 DISCUSSION

The results reported in the previous section are in agreement with the experiments reported by Gálvez et al. (2011). In fact, when the abundance of deuterated water is of the order of 0.1 per cent or less, the infrared spectra acquired on amorphous deposited samples have shown that the 4.1 μm vibrational mode band is not detectable, while the feature can be revealed in crystalline samples. Furthermore, we have shown that if a sample is deposited as a crystalline film and exposed to ion bombardment, the O–D stretching mode band disappears. This effect has to be ascribed to the ion-induced amorphization of water ice. The fit of the O–D normalized stretching band areas reported in Fig. 8 allowed us to obtain the cross section of the process $\sigma = 1.3\pm0.1$ 16u eV^{-1}. This value is comparable to the amorphization cross section obtained by Leto & Baratta (2003) for 30 keV H^+ on crystalline water ice, $k = 1.7\pm0.2$ molecule eV^{-1}, where 1 molecule = 18u.

In dense molecular clouds, water forms on the cold dust grains after grain surface reactions and its formation, as well as the formation of deuterated water, is regulated by the cloud characteristics. Several laboratory experiments have shown that water and deuterated water can be efficiently formed through the reaction of H and

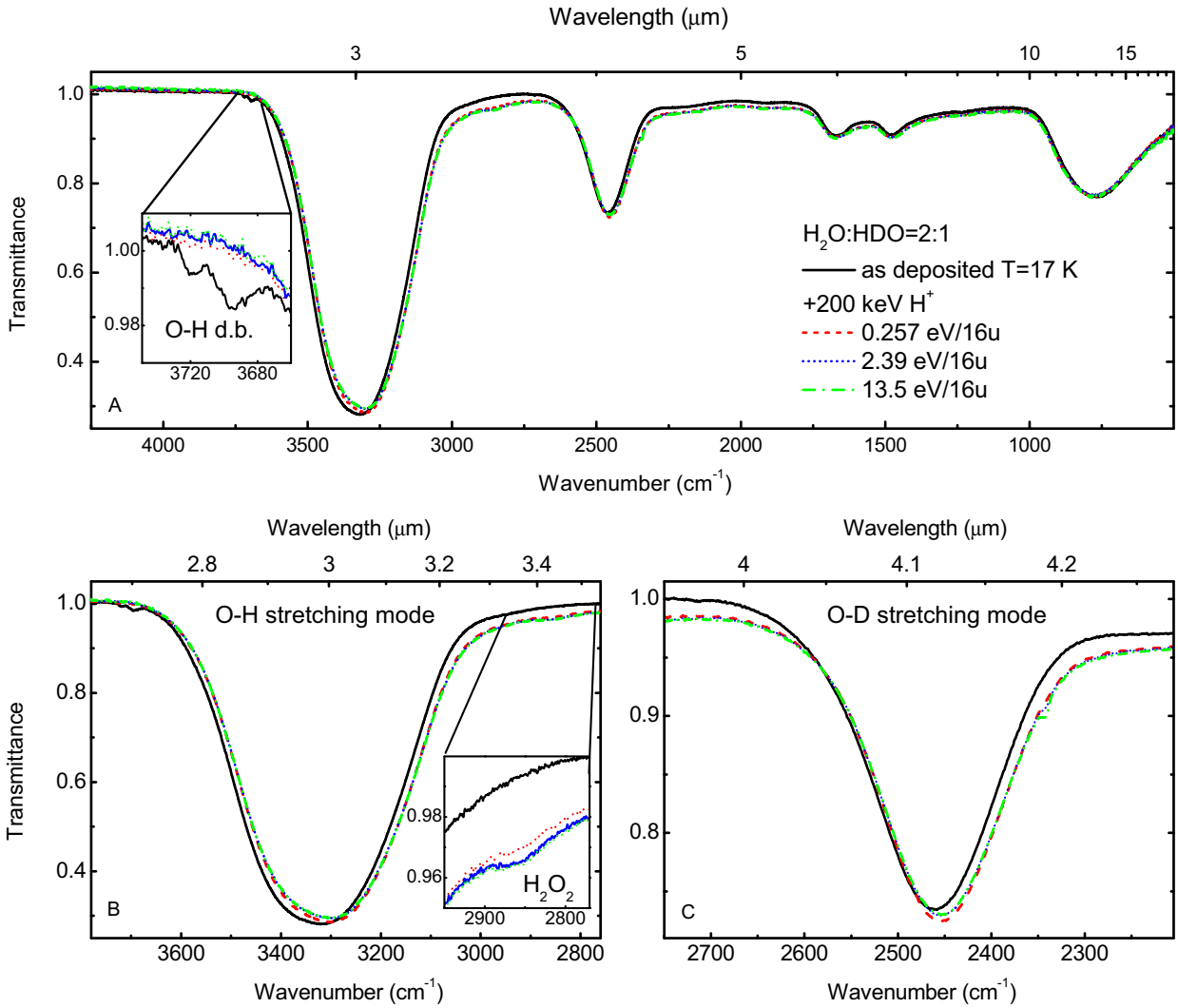

Figure 9. Infrared spectra in transmittance scale acquired during the irradiation of a H_2O:HDO =2:1 mixture with 200 keV H^+. Panel A: whole spectra; Inset: O–H dangling bonds; Panel B: O–H stretching mode band; Inset: H_2O_2 feature; Panel C: O–D stretching mode band.

D with O, O_2, and O_3 in icy grain mantle analogues (Hiraoka et al. 1998; Ioppolo et al. 2008; Oba et al. 2009; Mokrane et al. 2009; Dulieu 2011; Dulieu et al. 2011). Furthermore, the dust temperature can affect the HDO/H_2O ratio (e.g. Caselli & Ceccarelli 2012). According to Cazaux, Caselli & Spaans (2011), if the dust temperature is lower than 15 K, the HDO/H_2O ratio is predicted to be lower than 0.01 per cent, reflecting the HD/H_2 ratio close to the interstellar D/H ratio $\simeq 1.5 \times 10^{-5}$. If the temperature is above 15 K, the HDO/H_2O ratio can be as high as a few per cent.

Taking into account the work by Cazaux et al. (2011), the results reported in this work suggest that when water and deuterated water are formed on cold ($\leq$15 K) dust grains, the deuterated water abundance is too low and the 4.1 μm O–D stretching mode band could be detected only when HDO is embedded in crystalline icy mantles. On the other hand, when the dust grain temperature is above 15 K during water formation, the deuterated water/water ratio can be high enough to allow the O–D stretching mode band detection in amorphous ices also.

In the protostellar phase, the central object causes the presence of a thermal gradient in the surrounding matter, with the increasing temperature going towards the source. The thermal gradient determines whether molecules remain in the icy grain mantles or sublimate, thus dust grains that are further from the heating object may preserve their icy grain mantles. Furthermore, icy mantles closer to the heating source can undergo the amorphous-to-crystalline transition while those in the outer regions remain amorphous because in those regions the temperature is not high enough to cause their crystallization and the time required to undergo crystallization at lower temperature is higher than the age of these objects (e.g. Schmitt, Grimm & Greenberg 1988; Baragiola 2003).

In this scenario a correct estimation of the HDO/H_2O ratio requires the observations of both the O–H stretching mode band at 3.03 μm and the O–D stretching mode band at 4.1 μm. In fact the profile of the non-saturated 3.03 μm band gives an estimation of the fraction of crystalline ice along the line of sight (e.g. Leto & Baratta 2003), which in turn gives an estimation of the average temperature along the line of sight. As shown in Fig. 6 the ratio between the 3.03 and the 4.1 μm band area is independent of the sample temperature when the HDO concentration is of the order of few per cent while it strongly depends on the sample temperature when the concentration of HDO is of the order of 0.1 per cent or less.

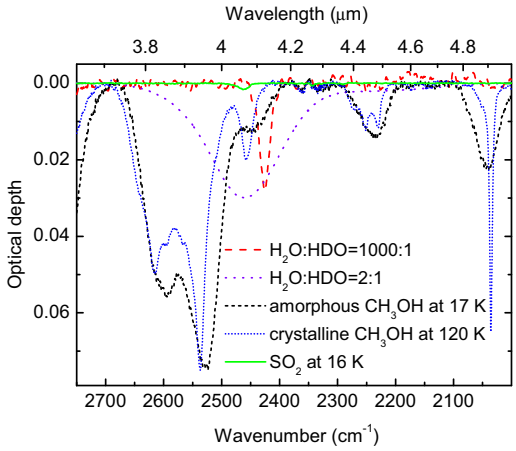

Figure 10. Transmittance spectra in optical depth scale (in the 4 μm region) of two different H_2O:HDO mixtures, CH_3OH and SO_2 ice samples. The optical depth of each feature has been scaled according to the value observed towards W33 A.

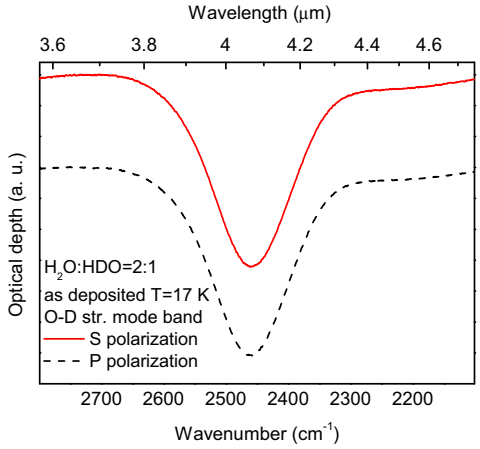

Figure 11. Infrared spectra acquired in S-polarization (red solid line) and P-polarization (black dashed line) on a H_2O:HDO =2:1 frozen mixture deposited at 17 K. The O–D stretching mode band profiles acquired in the two polarization modes are superimposable.

Infrared observations towards various star-forming regions have shown that solid-phase water is found both pure and in mixture with other species, such as CO and CO_2. In particular, about 10–20 per cent of CO_2 is observed within H_2O ice (e.g. Öberg et al. 2011). According to the experiments reported by Öberg et al. (2007), the presence of a small amount of CO_2 in ices should not significantly modify the results reported in this work.

To date, the presence and abundance of deuterated water in the solid phase of star-forming regions is still under debate. The main reason is due to the low amount of available data for the 4.1 μm spectral region. In fact, observations by means of ground-based infrared telescopes are hindered by the atmospheric CO_2 absorption. Thus, only space telescopes can be used to observe the O–D stretching mode band. Also, as we have shown in Fig. 10, the presence of other solid-phase interstellar molecule vibrational features close to the O–D stretching mode band frequency could drive to misleading considerations about the presence and the abundance of deuterated water in icy grain mantles. In particular, the contribution in the band intensity of the 4.1 μm band due to the presence of methanol and sulphur dioxide has to be taken into account in order to avoid overestimating the HDO abundance.

We expect that the higher sensitivity of the detectors on board the JWST, whose launch is scheduled in 2020, will allow to spread light about the presence of deuterated water together with other minor species that are thought to be present in icy grain mantles, and those which have not been observed yet. Also, the resolution of these detectors could allow to disentangle the O–D stretching mode band from those related to CH_3OH and SO_2.

Water ice is largely present in the Solar system in a number of surfaces of planets, moons, comets, and rings (e.g. Schmitt, de Bergh & Festou 1998). Its detection is mainly based on reflectance near-IR spectra. In fact, the spectrum of solid water shows two absorption features at about 2.0 and 1.5 μm (5000 and 6600 cm^{-1}; e.g. Grundy & Schmitt 1998; Gerakines, Bray & Davis 2005; Mastrapa & Brown 2006). In amorphous samples these features are smooth and symmetric, while in crystalline samples an additional feature appears at about 1.65 μm (6060 cm^{-1}). Laboratory experiments have shown that the relative intensity of this latter feature increases as the temperature of the crystalline sample decreases. Based on these results Grundy et al. (1999) have studied the possibility to use the 1.65 μm feature seen in reflectance spectra obtained by ground based observations to evaluate the surface temperatures on satellites of Jupiter, Saturn, and Uranus.

Gas phase deuterated water has been detected in various Solar system objects (e.g. Hartogh et al. 2011). According to current models, at the time of Solar system formation, water in the outer regions of the disc would preserve its original high D/H ratio from the molecular cloud (e.g. Hallis 2017). Thus it cannot be excluded that solid HDO mixed with H_2O is present on icy bodies (such as the satellites of Jupiter, Saturn and Uranus, and TNOs) in the outer Solar system. Recently, Altwegg et al. (2017) reported about the HDO and D_2O abundances in the coma of 67P/Churyumov–Gerasimenko measured by the ROSINA instrument on board the Rosetta spacecraft. The values they obtained suggest that the comet contains some material from the pre-solar disc that mostly remained unprocessed before accretion by the comet. In particular, the [D_2O]/[HDO] ratio is thought to give indications about the history of water in comets. Thus, deuterated water assumes a primary role in helping to reconstruct the Solar system history. Detection of solid HDO requires observations in the 4 μm spectral region, which are very challenging with present available instrumentation but which could be obtained in the near future with the JWST. The simultaneous observation of the 1.65 μm and 4.1 μm features will allow to better constrain the crystalline structure and the temperature of the ice and the H_2O:HDO ratio.

5 CONCLUSIONS

In this work we have presented a study on the profile of the O–D stretching mode band in various solid mixtures containing water and deuterated water. We have investigated the role of the dilution, of the structure of the sample (porous, amorphous, and crystalline) and of ion bombardment (200 keV H^+). We have found that the above parameters may influence the ratio between the O–D and the O–H stretching mode band.

Most of the information about solid-phase species and their abundances in space derives from the observations carried out by infrared telescopes. However, at present time the available astronomical spectra are not detailed enough to confirm the presence of deuterated water.

We expect that the JWST will provide us with new high resolution and high signal to noise ratio spectra in the line of sight to star forming regions and icy bodies in the Solar system. The comparison between observed and laboratory spectra will allow to better constrain the presence and the abundance of solid-phase deuterated water in astrophysical environments.

ACKNOWLEDGEMENTS

This work has been supported by the Italian Ministero dell'Istruzione, dell'Università e della Ricerca through the grant Progetti Premiali 2012-iALMA (CUP C52I13000140001).

REFERENCES

Aikawa Y. et al., 2012, A&A, 538, A57
Allamandola L. J., Sandford S. A., Tielens A. G. G. M., 1992, ApJ, 399, 134
Altwegg K., Balsiger H., Berthelier J. J. et al., 2017, Phil. Trans. R. Soc., A, 375, 20160253
Altwegg K., Balsiger H, Bar-Nun A. et al., 2015, Science, 347, 1261952
Baragiola R. A., 2003, Planet. Space Sci., 51, 953
Baratta G. A., Palumbo M. E., Strazzulla G., 2000, A&A, 357, 1045
Baratta G. A., Leto G., Spinella F., Strazzulla G., Foti G., 1991, A&A, 252, 421
Bennett C. J., Chen S. H., Sun B. J., Chang A. H. H. Kaiser R. I., 2007, ApJ, 660, 1588
Boogert A. C. A., Schutte W. A., Helmich F. P., Tielens A. G. G. M., Wooden D. H., 1997, A&A, 317, 929
Boogert A. C. A. et al., 2000, A&A, 353, 349
Boogert A. C. A., Blake G. A., Tielens A. G. G. M., 2002, ApJ, 577, 271
Boogert A. C. A. et al., 2008, ApJ, 678, 985
Boogert A. C. A., Gerakines P. A., Whittet D. C. B., 2015, ARA&A, 53, 541
Bossa J.-B., Isokoski K., de Valois M. S., Linnartz H., 2012, A&A, 545, A82
Brown R. H., Cruikshank D. P., Veverka J., Helfenstein P., Eluszkiewicz J., 1995, Neptune and Triton, University of Arizona Press, Tucson, p. 991
Butner H. M., Charnley S. B., Ceccarelli C., Rodgers S. D., Pardo J. R., Parise B., Cernicharo J., Davis G. R., 2007, ApJ, 659, L137
Calvin W. M., Clark R. N., Brown R. H., Spencer J. R., 1995. J. Geophys. Res., 100, 19041
Caselli P., Ceccarelli C., 2012, A&AR, 20, 56
Cazaux S., Caselli P., Spaans M., 2011, ApJ, 741, L34
Coutens A. et al., 2014, MNRAS, 445, 1299
Cruikshank D. P., Veverka J., Lebofsky L. A., 1984, Saturn, University of Arizona Press, Tucson, p. 640
Cruikshank D. P., Brown R. H., Calvin W. M., Roush T. L., Bartholomew M. J., 1995, Sol. Syst. Ices, 227, 579
Dartois E., 2005, Space Sci. Rev, 119, 293
Dartois E., d'Hendecourt L., 2001, A&A, 365, 144
Dartois E., Thi W.-F., Geballe T. R., Deboffle D., d'Hendecourt L., van Dischoeck E., 2003, A&A, 399, 1009
Dartois E. et al., 2013, A&A, 557, A97
Dartois E. et al., 2015, A&A, 576, A125
Dulieu F., 2011, in Cherninchero J., Bachiller R., eds., Proc. IAU Symp. 280, The Molecular Universe, Vol. 280, p. 405
Dulieu F., Amiaud L., Fillion J.-H., Matar E., Momeni A., Pirronello V., Lemaire J. L., 2007, in Lemaire J. L., Combes F., Diana S., eds., Molecules in Space and Laboratory, p. 79
Fulvio D., Sivaraman B., Baratta G. A., Palumbo M. E., Mason N. J., 2009, Spectrochim. Acta A, 72, 1007
Füri E., Marty B., 2015, Nat. Geosci., 8, 515
Gálvez Ó., Maté B., Herrero V. J., Escribano R., 2011, ApJ, 738, 133
Gerakines P. A., Schutte W. A., Greenberg J. M., van Dischoeck E. F., 1995, A&A, 296, 810
Gerakines P. A., Bray J. J., Davis A., Richey C. R., 2005, ApJ, 620, 1140
Gibb L., Whittet D. C. B., Boogert A. C. A., Tielens A. G. G. M., 2004, ApJS, 151, 35
Giguère P. A., Falk M., 1956, Can. J. Chem., 34, 1833
Grundy W. M., Schmitt B., 1998, J. Geophys. Res., 103, 25809
Grundy W. M., Buie M. W., Stanberry J. A., Spencer J. R., Schmitt B., 1999, Icarus, 142, 536
Hallis L. J., 2017, Phil. Trans. R. Soc. A, 375, 20150390
Hartogh P. et al., 2011, Nature, 478, 218
Hiraoka K., Miyagoshi T., Takayama T., Yamamoto K., Kihara Y., 1998, ApJ, 498, 710
Hudgins D. M., Sandford S. A., Allamandola L. J., Tielens A. G. G. M., 1993, ApJS, 86, 713
Ioppolo S., Cuppen H. M., Romanzin C., van Dishoeck E. F., Linnartz H., 2008, ApJ, 686, 1474
Jacq T., Jewell P. R., Henkel C., Walmsely C. M., Baudry A., 1990, A&A, 199, L5
Jenniskens P., Blake D. F., 1994, Science, 265, 753
Kama M. et al., 2013, A&A, 556, A57
Langer W. D., Penzias A. A., 1990, ApJ, 357, 477
Leto G., Baratta G. A., 2003, A&A, 397, 7
Leto G., Gomis O., Strazzulla G., 2005, Mem. Soc. Astron. Ital. Suppl., 6, 57
Madden W. G., Bergren M. S., McGraw R., Rice S. A., Sceats M. G., 1978, J. Chem. Phy., 69, 3497
Mastrapa R. M. E., Brown R. H., 2006, Icarus, 183, 207
Mokrane H., Chaabouni H., Accolla M., Congiu E., Dulieu F., Chehrouri M., Lemaire J. L., 2009, ApJ, 705, L195
Moore M. H., Hudson R. L., 1992, ApJ, 401, 353
Moore M. H., Hudson R. L., 2000, Icarus, 145, 282
Morrison D., Johnson T. V., Shoemaker T. M., Soderblom L. A., Thomas P., Veverka J., Smith B. A., 1984, Saturn. University of Arizona Press, Tucson, p. 609
Nagy Z. et al., 2017, A&A, 599, A22
Nash D. B., Betts B. H., 1995, Sol. Syst. Ices, 227, 607
Oba Y., Miyauchi N., Hidaka H. et al., 2009, ApJ, 701, 464
Öberg K. I., Fraser H. J., Boogert A. C. A., Bisschop S. E., Fuchs G. W., van Dishoeck E. F., Linnartz H., 2007, A&A, 462, 1187
Öberg K. I., Boogert A. C. A., Pontoppidan K. M., van den Broek S., van Dishoeck E. F., Bottinelli S., Blake G. A., Evans N. J. II, 2011, ApJ, 740, 109
Palumbo M. E., 2006, A&A, 453, 903
Palumbo M. E., Baratta G. A., 2000, A&A, 361, 298
Palumbo M. E., Geballe T. R., Tielens A. G. G. M., 1997, ApJ, 479, 839
Parise B., Simon T., Caux E., Dartois E., Ceccarelli C., Rayner J., Tielens A. M. M. A., 2003, A&A, 410, 897
Pineda J. E., Caselli P., Goodman A. A., 2008, ApJ, 679, 481
Raut U. et al., 2007, J. Chem. Phys., 126, 4511
Rowland B., Fisher M., Devlin J. P., 1991, J. Chem. Phys., 95, 1378
Sandford S. A., Allamandola L. J., 1993, ApJ, 417, 815
Schmitt B., Grimm R., Greenberg M., 1988, in Proc. 22nd Elsab Symposium on Infrared Spectroscopy in Astronomy, Salamanca, p. 213
Schmitt B., de Bergh C., Festou M., 1998, Solar System ices. Kluwer Academic Publisher, Dordrecht, p. 826
Schutte W. A., Gerakines P. A., van Dishoeck E. F., Greenbergand J. M., Geballe T. R., 1994, in Nenner I., ed., AIP Conf. Proc. Vol. 312, Molecules and Grains in Space, Am. Inst. Phys., New York, p. 73
Strazzulla G., Johnson R. E., 1991, Irradiation Effects on Comets and Cometary Debris, Comets in the post-Halley era. Springer Netherlands, Dordrecht, p. 243
Strazzulla G., Leto G., Gomis O., Satorre M. A., 2003, Icarus, 164, 163
Sun Q., 2013, Chem. Phys. Lett., 568, 90
Teixeira T. C., Devlin J. P., Buch V., Emerson J. P., 1999, A&A, 347, L19
Thomas P., Veverka J., Dermott S., 1986, Satellites. University of Arizona Press, Tucson, p. 802
Turner B. E., Zuckerman B., Fourikis N., Morris M., Palmer P., 1975, ApJ, 198, L125
Urso R. G., Scirè C., Baratta G. A., Compagnini G., Palumbo M. E., 2016, A&A, 594, A80

Urso R. G., Scirè C., Baratta G. A., Brucato J. R., Compagnini G., Kaňuchová Z., Palumbo M. E., Strazzulla G., 2017, Phys. Chem. Chem. Phys., 19, 21759
Wiener R. N., Nixon E., 1956, J. Chem. Phys., 25, 175
Zheng W., Jewitt D., Kaiser R. I., 2006, ApJ, 639, 534
Ziegler J. F., Biersack J. P., Ziegler M. D., 2008, The Stopping and Range of Ions in Solids. Pergamon Press, New York, p. 321

This paper has been typeset from a TEX/LATEX file prepared by the author.